

Article

Collaborative Multi-Robot Formation Control and Global Path Optimization

Di Liang¹, Zhongyi Liu^{1,*} and Ran Bhamra²¹ School of Mechanical and Engineering, Shenyang University, Shenyang 110044, China; liangdi@syy.edu.cn² School of Business and Management Royal Holloway, University of London, Egham TW20 0EX, UK; ran.bhamra@rhul.ac.uk

* Correspondence: liuzhongyy10133@163.com; Tel.: +86-158-4069-8891

Abstract: For multi-robot cooperative formation and global path planning, we propose to adjust the repulsive field function and insert a dynamic virtual target point to solve the local minima and target unreachability problems of the traditional artificial potential field (APF) method. The convergence speed and global optimization accuracy of ant colony optimization (ACO) are improved by introducing improved state transfer functions with heuristic information of the artificial potential field method and optimizing the pheromone concentration update rules. A hybrid algorithm combining APF and improved ACO is used to calculate an optimal path from the starting point to the end point for the leader robot. A cooperative multi-robot formation control method combining graph theory and consistency algorithm is proposed based on path planning of the leader robot. Taking AGVs in a logistics distribution center as an example, the feasibility of the improved algorithm and its effectiveness in solving the multi-robot path planning problem are verified.

Keywords: artificial potential field; ant colony optimization; graph theory; multi-robot formation control; consistency algorithm



Citation: Liang, D.; Liu, Z.; Bhamra, R. Collaborative Multi-Robot Formation Control and Global Path Optimization. *Appl. Sci.* **2022**, *12*, 7046. <https://doi.org/10.3390/app12147046>

Academic Editors: Mujahed Al-Dhaifallah and Ibrahim Aljamaan

Received: 10 June 2022

Accepted: 8 July 2022

Published: 12 July 2022

Publisher's Note: MDPI stays neutral with regard to jurisdictional claims in published maps and institutional affiliations.



Copyright: © 2022 by the authors. Licensee MDPI, Basel, Switzerland. This article is an open access article distributed under the terms and conditions of the Creative Commons Attribution (CC BY) license (<https://creativecommons.org/licenses/by/4.0/>).

1. Introduction

In the context of the continuous development and improvement of artificial intelligence theory, mobile robots have become more intelligent and autonomous, capable of replacing or assisting humans to complete dangerous, complex, and boring work. Therefore, mobile robots are widely used in industrial production, military operations, medical services, construction, and other fields. As a crucial technology for mobile robots, navigation technology fundamentally affects the path planning capability of mobile robots, determines whether they can identify and avoid obstacles, and calculates the best route to complete the task in the current working environment, quickly and accurately [1]. With the rapid development of various industries, single robots are no longer able to meet the demands of enterprises in terms of production, cost, and service efficiency, etc. Therefore, people are improving the performance of single robots and working on the research of multi-robot formation control to accomplish tasks that cannot be done by a single robot.

The working environment of mobile robots is divided into static and dynamic [2]. In the former, the start and end points and obstacles are known and unchanged; in the latter, the moving path has to be calculated in real time based on the feedback information from sensors, since the start and endpoints and obstacles are dynamically changed. Path planning is further divided into local and global, depending on how much information the robot has about the environment. For the former, the environmental information is opaque, and the robot acquires information through sensors such as the position and geometric properties of obstacles, which are processed and computed at high speeds to perform obstacle avoidance. In the case of the latter, a path for the robot is planned in a known environment, and its accuracy depends on the degree of environmental information

acquisition. The aim of this study is the application of multi-robot formations in global path planning in a static environment.

Many scholars focus on mobile robot path planning, and, so far, a large number of control optimization methods have been proposed. These include the Dijkstra algorithm [3], genetic algorithm [4], firefly algorithm [5], A* algorithm [6], artificial potential field method [7], RRT algorithm [8], neural network algorithm [9], etc. However, due to their own defects, these heuristic algorithms often cannot complete the task satisfactorily. For example, it takes the A* algorithm a long time to find a better path by traversing all reachable nodes [10]. The RRT algorithm is overly stochastic and has a high number of redundant nodes and path inflection points [11].

The study of heuristic algorithm improvement strategies for path planning problems has become popular nowadays. The artificial potential field method is one of the classical algorithms applied to path planning, but suffers from the defects of not being able to reach the target point and easily falling into the local optimum [12]. In response, scholars have taken a series of measures to address the above issues. Ulises et al. [13] proposed a membrane-evolving APF to find parameters that can generate feasible safe paths. Bence et al. [14] have extended the APF through the motion characteristics of animals to enhance the human-robot interaction. Sudan et al. [15] proposed an improved APF for solving the obstacle avoidance problem of multiple robots. Hou et al. [16] introduced the distance between the robot and the target point into the repulsive field function, avoiding the local optimization problem.

The ACO is also a classical path planning method with the advantages of good feedback information and distributed computation [17]. However, due to the limitation of its own mechanism, the computational overhead is large and the convergence speed is slow in the process of finding the optimal path [18]. Viswanathan et al. [19] used the sigmoid function to change the ant colony pheromone update mechanism and reduce the computational cost. Tao et al. [20] introduced key obstacle influence factors into the heuristic information, which changed the pheromone volatility rate and improved the convergence speed of the ACO. Luo et al. [21] constructed the initial pheromone with unequal allocation and introduced a dynamic penalty method to improve the ACO. Han et al. [22] proposed an ACO with faster convergence and better obstacle avoidance. Jiao et al. [23] improved the search speed of the algorithm using multiple ant colony partitioning and a cooperative mechanism. Liang and Wang [24] combined GA with ACO to improve the robustness and the solution quality. Gao et al. [25] proposed a new pheromone diffusion gradient formula to accelerate ACO.

The above improvement strategies were optimized for the disadvantages of APF and ACO, respectively, but the trade-off between path optimization and computational cost still faced a tough choice. Some scholars started to combine the advantages of ACO and APF to find a new solution strategy.

Liu et al. [26] optimized the initial pheromone of ACO with an improved APF algorithm to improve the directionality of ants in the early stage of path search. Chen et al. [27] combined APF and ACO to improve the convergence of the algorithm. Liu et al. [28] used APF to optimize the pheromone matrix of the ACO to improve the algorithm performance and search efficiency. Park et al. [29] used the improved APF ensemble to optimize the setting of heuristic information and volatile factors of ACO to avoid the problem of falling into a local optimum. Although the above studies have improved the defects of the single algorithm to some extent, APF-ACO still has the problems of large computation and poor performance of the optimal solution due to the influence of APF and ACO's own mechanism [30].

Therefore, a new APF-ACO is proposed in this paper, which improves the convergence speed and the optimization-seeking accuracy of the basic algorithm and can solve the robot path planning problem as well. However, a single path planning algorithm does not enable robots to form effective formations and is less controllable, and multi-robot formation path planning has also attracted the attention of many scholars.

Without considering information delay, Peng et al. [31] investigated distributed formation control of multiple mobile robots based on graph theory and Lyapunov theories. Pan et al. [32] proposed a virtual spring path planning and formation control method for multi-robot systems. Wu et al. [33] investigated an observer-based approach to robot formation control. Doaa et al. [34] combined graph theory with ant colony algorithms and applied them to the study of path planning for robot formations. Liu et al. [35] applied a third-order control protocol to implement the control of robot formations. Wang et al. [36] proposed an optimization model with multi-stage consistency improvement to solve the problem of decision making in the absence of knowledge. Henrik and Eberhard [37] combine algebraic graph theory with distributed control to study the robot formation framework. Yan et al. [38] proposed a formation consistency control method for mixed-order systems with switching topology to improve the stability of formation control.

The studies mentioned above have investigated the construction and control of robot formations using methods such as graph theory and consistency control, but relatively few studies have combined the two. In this study, we use a graph-theoretic approach for robot formation construction and a consistency control approach for maintaining the formation.

In summary, this paper investigates the global path planning problem for multi-robot formations in static environments. The main contributions are as follows: (1) adjusting the repulsive field function and introducing dynamic virtual target points to solve the problem that APF is prone to local optimum and target unreachability; (2) changing the concentration of ant colony pheromone and improving the state transfer function with the improved APF repulsive field function to improve the search efficiency and solve the problems of local optimum and slow convergence; (3) using graph theory and the consistency control method to build the formation of robots and improve the stability of formation control.

The remainder of this article is organized as follows. Firstly, the theoretical foundations and hypotheses are presented. Secondly, our research design and methodology are described. Following that, the analysis, results, and implications of our findings are discussed. Furthermore, an application of the improved ACO is shown with the case study on the AGV formation path planning. Finally, conclusions and directions for future research are presented.

2. Improved Artificial Potential Field Method

2.1. Classical Artificial Potential Field Method

In the APF, the obstacle and the target point generate repulsive and gravitational potential fields, respectively, which act simultaneously on the robot to make it move safely from the starting point to the target point without collision.

The robot path planning problem is studied in two dimensions, and the robot is regarded as a particle. Assuming that its position in the potential field is $W_1 = (x, y)$, then the position of the target point is $W_2 = X_N = [x_n, y_n]$, and the gravitational force on the robot is as follows:

$$F_G(X) = -\Delta \left[\frac{1}{2} k (X - X_n)^2 \right] = k \varepsilon_1 \alpha_1 \quad (1)$$

where $k_g > 0$ is the gravitational gain coefficient; α_1 and ε_1 represent the unit vector and linear distance of the robot from the target point in the potential field, respectively, where $\varepsilon_1 = \|X - X_n\|$. The robot is subject to the repulsive force function of the obstacles in the environment as follows:

$$F_Z(x) = k_z \left(\frac{1}{\mu} - \frac{1}{\mu_0} \right) \frac{1}{\mu^2} \cdot \frac{\partial \mu}{\partial X} \quad (2)$$

where $k_z > 0$ is the repulsive gain coefficient of the function; μ is the distance between the robot and the obstacle; μ_0 is the range of the obstacle, $\mu \leq \mu_0$. The direction and magnitude of the robot's motion in the potential field depends on the combined force $F(X)$:

$$F(X) = F_G(X) + F_Z(x) \quad (3)$$

2.2. Repulsive Potential Field Function Adjustment

To solve the defect that the target is not reachable during the robot movement, the repulsive potential field function is now adjusted as Equation (4).

$$U_{rep}(x) = \begin{cases} \frac{1}{2}\eta\left(\frac{1}{\rho(X, X_0)} - \frac{1}{\rho_0}\right) \cdot \rho^n(X, X_0), & \rho(X, X_0) \leq \rho_0 \\ 0, & \rho(X, X_0) > \rho_0 \end{cases} \quad (4)$$

where $\rho(X, X_0)$ is the Euclidean distance between the robot and the obstacle, η is the repulsion gain coefficient, and n is the regulation constant. The negative gradient of the repulsive field function can be obtained according to Equation (4), and the improved APF repulsive function is as follows:

$$F_{rep}(X) = -\Delta[U_{rep}(X)] \quad (5)$$

$$\Delta[U_{rep}(X)] = \begin{cases} -(F_{rep1} + F_{rep2}), & \rho(X, X_0) \leq \rho_0 \\ 0, & \rho(X, X_0) > \rho_0 \end{cases} \quad (6)$$

where

$$F_{rep1}(X) = \eta\left(\frac{1}{\rho(X, X_i)} - \frac{1}{\rho_0}\right) \cdot \frac{\rho^n(X, X_g)}{\rho^2(X, X_i)} \quad (7)$$

$$F_{rep2}(X) = \frac{n}{2}\eta\left(\frac{1}{\rho(X, X_i)} - \frac{1}{\rho_0}\right) \cdot \rho^{n-1}(X, X_g) \quad (8)$$

From the above equation, the repulsive force $F_{rep1}(X)$ decreases to 0 when the robot moves toward the target point; the gravitational force $F_{rep2}(X)$ gradually increases when $0 < n < 1$. This ensures that the robot can reach the specified position even if there is an obstacle near the target point. In this case, the combined force on the robot is given by Equation (9).

$$F = F_a + \sum_{i=1}^m F_{rep,i} \quad (9)$$

where m is the number of effective obstacles. Assuming that the combined force F is at an angle θ with the x -axis, and k is the coordinate point of path, the next coordinate (x_{k+1}, y_{k+1}) , at which the robot moves, is calculated as follows, where l is the position shift length of the robot:

$$\begin{cases} x_{k+1} = x_k + l \cdot \cos \theta \\ y_{k+1} = y_k + l \cdot \sin \theta \end{cases} \quad (10)$$

2.3. Add Virtual Target Points

The step length of the robot is set to 5. When the consecutive step length is less than βl , $\beta \in [2, 4]$, the robot is judged whether it falls into local optimum by adjusting β . When the robot falls into the local optimum, the obstacle information is stored. Take the line between obstacles and destination as the center, and the side with more obstacles is the effective obstacle. The position of the virtual sub-target is calculated according to Equation (11):

$$\begin{cases} x_t = x_b + \beta_1 \cdot \sin n(x_g - x) \\ y_t = y_b + \beta_2 \cdot \sin n(y_g - y) \end{cases} \quad (11)$$

where (x, y) , (x_g, y_g) describe the current positions of the robot and the target point, respectively, (x_b, y_b) is the position of the effective obstacle, and β is the adjustment factor. By continuously changing the virtual target point, the robot jumps out of the locally optimal trap and then withdraws the virtual sub-target, allowing the robot to continue intermittent route planning under the original combined force.

3. Improved Global Path Planning with Ant Colony Algorithm

3.1. Classical Ant Colony Algorithm

The ACO achieves optimal search of paths through information probability selection and pheromone identification between ant colonies and their environment. The probability of the k th ant choosing the next node location at the intersection is as follows:

$$P_{ij}^k = \begin{cases} \frac{[\tau_{ij}(t)]^\alpha [\eta_{ij}]^\beta}{\sum\limits_{j \in \text{allowed}_k} [[\tau_{ij}(t)]^\alpha [\eta_{ij}]^\beta]}, & j \in \text{allowed}_k \\ 0, & \text{otherwise} \end{cases} \quad (12)$$

$$\eta_{ij} = \frac{1}{d_{ij}} \quad (13)$$

where allowed_k is the k th ant selectable node, α is the pheromone heuristic factor; β is the desired heuristic factor, τ_{ij} is the pheromone concentration of path (i, j) , η_{ij} is the heuristic information, and d_{ij} is the Euclidean distance between the current node i and the node j to be selected. The pheromone update rule is as follows:

$$\tau_{ij}(t+1) = (1 - \rho) \cdot \tau_{ij}(t) + \Delta\tau_{ij}(t, t+1) \quad (14)$$

$$\Delta\tau_{ij}(t, t+1) = \begin{cases} \frac{Q}{L_k}, & (i, j) \in P_k(\text{begin}, \text{end}) \\ 0, & \text{otherwise} \end{cases} \quad (15)$$

where $\rho \in (0, 1)$ is the pheromone volatility coefficient, $\Delta\tau_{ij}(i, j)$ is the pheromone increment from node i to node j , Q is the pheromone intensity; L_k is the path length of the k th ant in one cycle, and $P_k(\text{begin}, \text{end})$ is the path taken by ant k from the starting point to the end point.

3.2. Improved Pheromone Concentration Update Rules

When an ant passes a node, the pheromone change rule at that point is as follows:

$$\tau_{ij}(t) = (1 - \lambda)\tau_{ij}(t) + \lambda\tau_0 \quad (16)$$

where λ is the local pheromone volatility coefficient, $\lambda \in (0, 1)$; τ_0 is a very small constant; and by making $\tau_{ij}(t)$ equal to the limit value, the algorithm will avoid stagnation when $\tau_{ij}(t)$ exceeds the limit value.

The update rules for pheromone concentration according to the quality ant update is as Equation (17):

$$\tau_{ij}(t+1) = (1 - \rho)\tau_{ij}(t) - \varepsilon \frac{L_{\text{worst}}}{L_{\text{best}}} \quad (17)$$

where ε is the introduced parameter, $\varepsilon \in (0, 1)$, and L_{worst} and L_{best} are the lengths of the paths taken by the worst and best ants, respectively.

If the algorithm falls into a local optimum for a consecutive iteration T , it is automatically adjusted by the volatility factor ρ , as follows:

$$\rho(t+1) = \begin{cases} \gamma \cdot \rho(t), & \rho(t) \geq \rho_{\min} \\ \rho_{\min}, & \text{otherwise} \end{cases} \quad (18)$$

where γ is the global pheromone decrement factor, $\gamma \in (0, 1)$, and ρ_{\min} is the minimum pheromone volatility factor.

3.3. Improved State Transfer Function

The basic ACO uses a uniform distribution of initial pheromone concentration, which leads to a slow convergence rate. Therefore, in this paper, a higher initial value of pheromone concentration is determined with an improved APF, and then the next path

point direction is determined with virtual ensemble to improve the accuracy of planning direction. After introducing the heuristic information of the improved APF, the new state transfer function is shown in Equation (19):

$$P_{ij}^m(t) = \begin{cases} \frac{[\tau_{ij}(t)]^\alpha [\eta_{ij}(t)]^\beta [\eta_F(t)]^\gamma}{\sum_{s \in \text{allowed } A_m} [\tau_{ij}(t)]^\alpha [\eta_{ij}(t)]^\beta [\eta_F(t)]^\gamma}, & s \in \text{allowed } A_m \\ 0, & \text{else} \end{cases} \quad (19)$$

After establishing the grid model and setting the environment information, the flowchart of the operation of the improved ant colony algorithm is as shown in Figure 1.

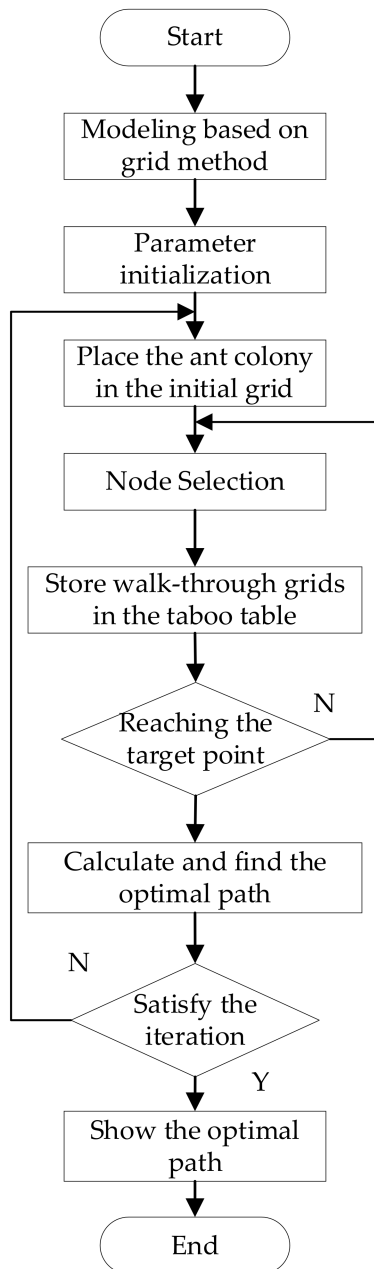


Figure 1. The flow chart of the improved ant colony algorithm.

3.4. Experimental Analysis of Global Path Planning Simulation

3.4.1. Parameter Setting

In order to verify the performance and the improvement effect of the improved ACO in this paper, a comparative simulation with the traditional ACO in two raster environments with different levels of complexity is performed.

A reasonable combination of parameters in the ant colony algorithm affects the optimal solution of path planning, and the values of each parameter are currently determined mainly by simulation experiments and empirical selection of multiple parameter combinations for comparison. In this paper, five different values are selected in the range of the main parameter variations according to empirical methods. A set of default parameter values is set as $\alpha = 1$, $\beta = 6$, and $\rho = 0.1$. To improve the rationality, different parameter combinations were set up by the single-variable control method, and 10 simulations were performed for each parameter combination in a 10×10 raster environment. The mean values of the simulation results were compared to select the best parameter combination.

The experimental results in Table 1 yield a range of optimal values for each major parameter, with α optimal around 1, β optimal around 6, and ρ optimal around 0.1. The specific experimental parameters were set as shown in Table 2, and this combination of parameters was followed in the subsequent study.

Table 1. Parameter selection.

Parameter	Parameter Experimental Comparison Values				
α	0	0.5	1	2	4
Path length mean/m	20.28	17.36	15.32	17.28	15.48
β	0	3	6	7	10
Path length mean/m	19.34	18.13	15.64	17.41	19.85
ρ	0.1	0.3	0.5	0.7	0.9
Path length mean/m	16.10	18.43	19.68	19.80	21.32

Table 2. Experimental parameter setting.

Parameter	N_{max}	M	α	β	ρ	Q
Value	50	30	1	6	0.1	10

3.4.2. 10×10 Static Environment Simulation Results Analysis

In this experiment, Matlab was used as the experimental platform, and 10×10 scale simple and complex grid obstacle environments were set respectively. The related parameter settings are shown in Table 2. The image shows that the obstacle distribution in simple environment is less, and the optimal path can be obtained before and after the ant colony algorithm is improved. However, a comparison between Figures 2 and 3 shows that the improved optimal path is smoother and shorter, the path length is 12.7280, and the algorithm tends to stabilize faster by 46.4%.

As shown in Figures 4 and 5, the search difficulty increases as the density of obstacle distribution in complex environment increases, and the path branch points become more frequent. The improved ACO still performs better than the classical ACO with the shortest path of 14.4854, and the speed of algorithm convergence to stability is improved by 41.4%. The above experimental results show that the improved ACO based on artificial potential field has significant advantages in the speed, and the results of optimal path search compared with the traditional ACO.

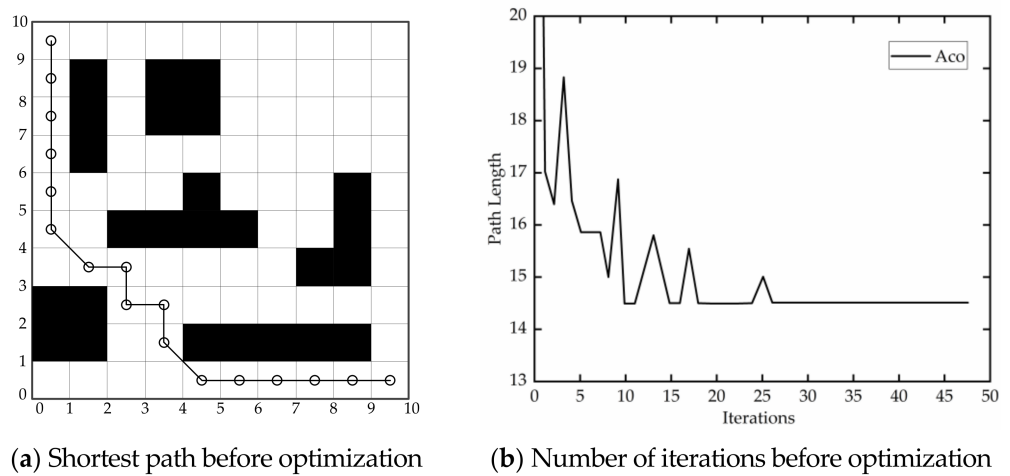


Figure 2. Path planning using basic ACO in the simple grid map.

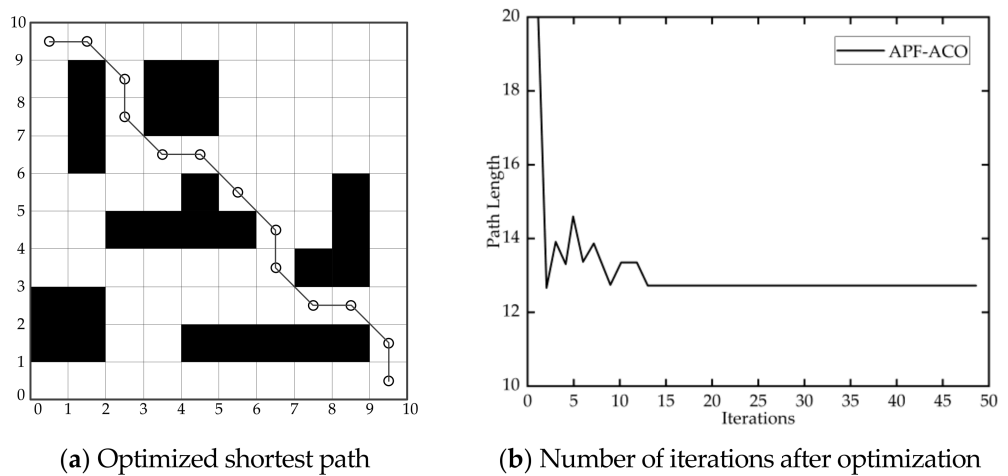


Figure 3. Path planning using improved ACO in the simple grid map.

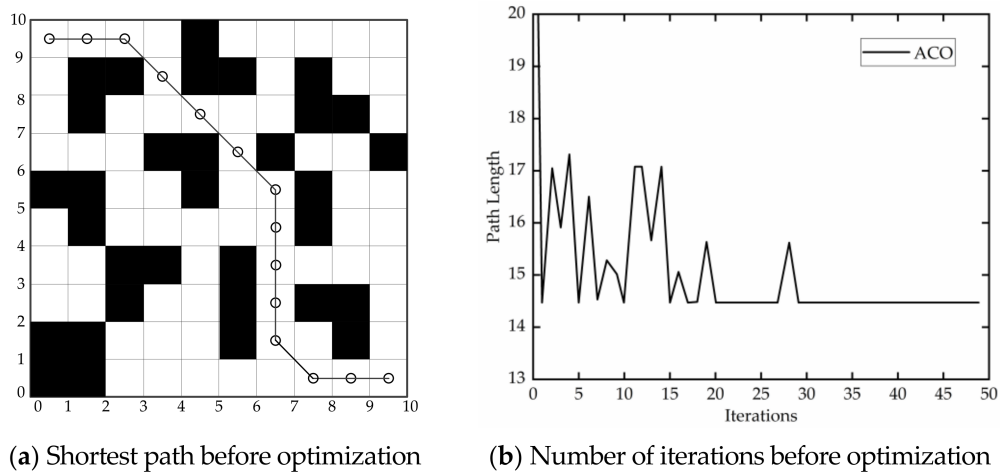


Figure 4. Path planning using basic ACO in the complex grid map.

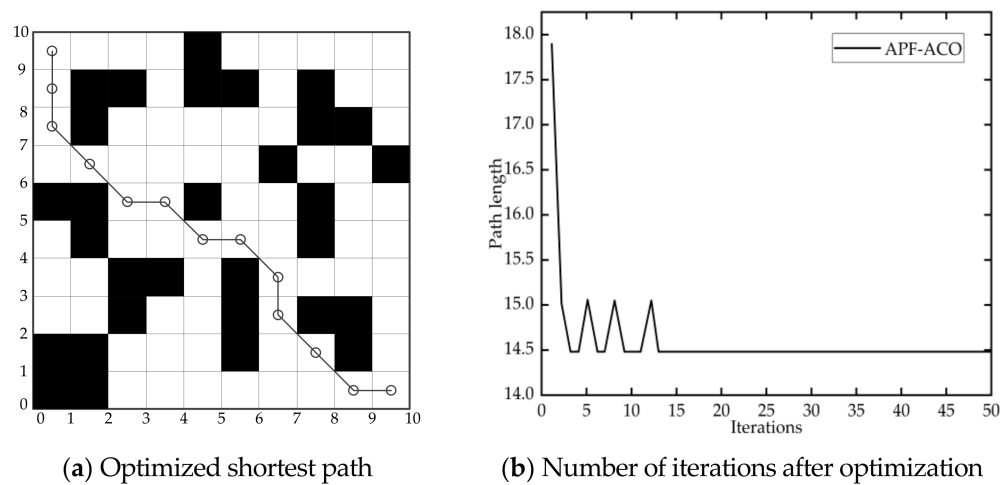


Figure 5. Path planning using improved ACO in the complex grid map.

The comparison of the results before and after algorithm improvement in two environments are shown in Table 3.

Table 3. Comparison of ACO and APF-ACO.

	ACO		APF-ACO	
	Best Path	Iterations	Best Path	Iterations
Simple map	14.5721	27	12.7280	13
Complex map	14.7286	29	14.4854	14

4. Global Path Planning for Multi-Robot Formations

4.1. Graph Theory

The robot formation problem can be viewed as how the graph topology interacts with the local feedback control protocols of the nodes to generate the overall behavior of the interconnected nodes. The topology diagram can be defined as $D(V, E)$, where $V = \{v_1, v_2, \dots, v_N\}$ denotes the set of N nodes; E is the set of edges. Assume that the graph is a simple directed graph $(v_i, v_j) \notin E$ and there are no redundant edges between the same nodes. The element (v_i, v_j) in the set E in the formation represents the robots whose information flows from node v_j robot to node v_i . The out-degree d_i^o of a node robot represents the number of edges with it as the data sender, and the in-degree d_i represents the number with it as the data receiver.

Determine the weights of the edges as a_{ij} , and then represent the graph as a matrix $A = [a_{ij}]$. When $(v_i, v_j) \notin E$, $a_{ij} = 1$; otherwise $a_{ij} = 0$.

$$d_i = \sum_{j=1}^N a_{ij}, \quad d_i^o = \sum_{j=1}^N a_{ji} \quad (20)$$

Next, a diagonal matrix $D = \text{diag } d_i$ and a Laplace matrix $L = D - A$ are defined. The eigenvalues of L are analyzed and the Jordan form of the Laplace matrix is defined as follows:

$$L \equiv M J M^{-1} \quad (21)$$

where the Jordan Matrix J and the transformation matrix M are

$$J = \begin{pmatrix} \lambda_1 & 1 & & \\ & \lambda_2 & 1 & \\ & & \ddots & 1 \\ & & & \lambda_N \end{pmatrix},$$

$$M = [v_1, v_2, \dots, v_N]$$

where eigenvalues λ_i and the right eigenvectors v_i of M satisfy $(\lambda_i I - L)v_i = 0$, and I is the unit matrix. The left eigenvector w_i of M satisfies $w_i(\lambda_i I - L) = 0$.

4.2. Formation Control Based on Consistency Method

The formation structure in this study is a distributed control structure in a navigator-follower formation, and the formation control is achieved through the combination of graph theory and consistency algorithms. The first-order continuous system model of the formation system is as Equation (22).

$$\dot{x} = u_i \quad (22)$$

x_i, u_i denote the state quantity and the input quantity of the node, respectively, $x_i, u_i \in R^n$, and n denotes the dimension of the state quantity. Ideally, the control inputs are as Equation (23):

$$u_i = \sum_{j \in N_i} a_{ij}(x_j - x_i) \quad (23)$$

where a_{ij} is the adjacency matrix element of the formation and N_i is the set of neighbors of member i . After introducing Equations (22) and (23) into the global state vector $x = [x_1, x_2, \dots, x_n]^T \in R^n$, the global dynamic relations are obtained as follows:

$$\dot{x} = -Dx + Ax = -Lx \quad (24)$$

Equation (24) shows that the closed-loop dynamic properties of the formation depend on the matrix L . The $-L$ eigenvalues are all located in the left half-plane of the complex plane when and only when the topological graph G of the formation has a spanning tree, so that Equation (23) ensures that the system achieves consistency and the final state values are as follows:

$$c = \sum_{i=1}^N p_i x_i \quad (25)$$

Equation (22) can be discretized as:

$$x_i(k+1) = x_i(k) + u_i(k) \quad (26)$$

In this study, assuming that the navigator leads the other robots from the starting point towards the target point, ideally the algorithm for the followers in the formation takes the following form:

$$x_i(k) = \varepsilon \sum a_{ij}(x_j(k) - x_i(k) - r_{ij}(k)) \quad (27)$$

where $\varepsilon > 0$, r_{ij} denotes the relative positions of robot i and robot j . The control equation for leader N is:

$$u_N(k) = m + kD(k) + \sum_{i \in N_i} a_{Ni} r_{Ni}(k) \quad (28)$$

m and k are constants, and $D(k)$ is the distance between the leader and the target point at moment k . The velocity is affected by the neighboring nodes and the distance from the target point.

4.3. Formation Control Simulation Analysis

According to previous research, this section sets up a single leader–single follower structure formation, and the formation is formed with the following robot in the coordinate system of the leader robot, $D = (-20, -30)$. Other parameters are set as follows: $\Delta = 10$, $u_1^d = 1.5$, $\chi(\cdot) = \frac{3}{\pi} \arctan(\cdot)$.

Figure 6 illustrates the simulation results. The formation control is stable during the robot moving to the destination, and, while there is a little bit of error in the change of direction phase, it is within the controllable range.

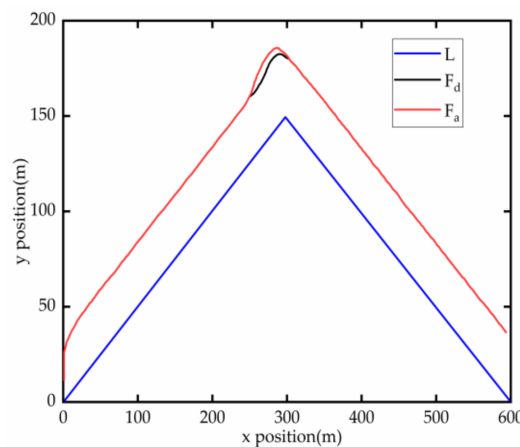


Figure 6. Single leader and single follower.

For a single leader–two-follower formation, the starting point position is set to $L(80, 50)$, $F_1(0, 100)$, $F_2(0, 0)$, and the desired formation is $D[100, 100, 100]$. The leader robot travels to the first target point $(300, 500)$, and then travels to the second target point $(600, 50)$. The follower robot follows the leader robot for movement and maintains the formation. The parameter k is taken as 0.2, and the simulation results are shown in Figure 7.

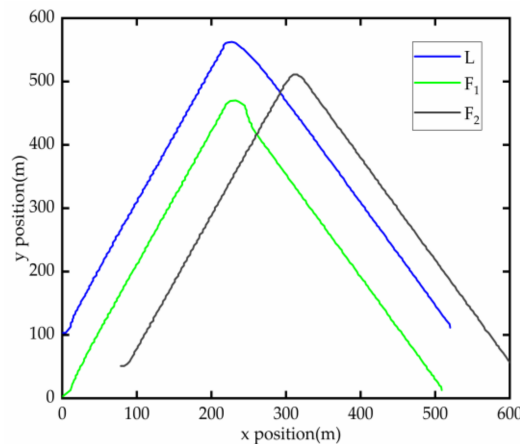


Figure 7. Single leader and double follower.

5. Application to the AGV Case

This section applies the above strategies to logistics company A, uses the grid method to discretize the environmental information of its warehouse, sets the shelves and other facilities as obstacles, configures the environmental information according to their locations and sizes, and uses the improved ant colony algorithm to plan a shortest path from the starting point to the end point for the AGV formation. For the leader AGV, start point coordinates are $(1.8, 48.5)$, and end point coordinates are $(49.5, 0.5)$. For the follower

AGV, start point coordinates are (1.5, 49.5), and end point coordinates are (49.5, 1.5). The simulation result of single leader formation is shown in Figure 8.

As for the single leader–two-follower AGV shown in the Figure 9, the starting point positions of the leader AGV and follower AGV 1 are the same as above, and the starting coordinates of the follower AGV 2 are (0.5, 48.5).

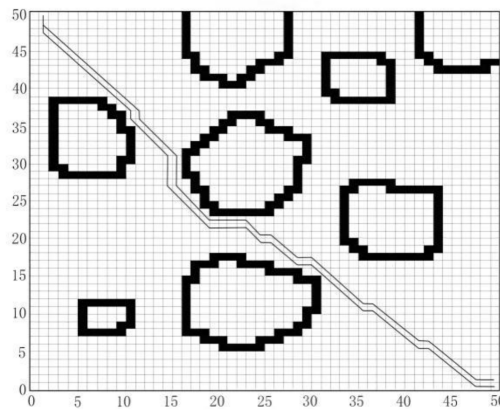


Figure 8. Path planning simulation diagram of single leader and single follower.

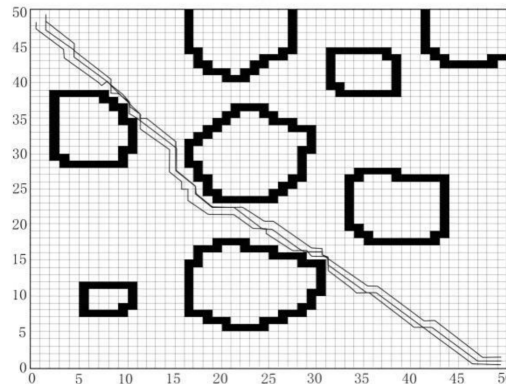


Figure 9. Path planning simulation diagram of double leader and single follower.

The simulation results describe that no matter singleleader–single follower or singleleader–two-follower, AGV formation can be maintained well and reach the end position smoothly without collision.

6. Conclusions

In response to the local minima and target unreachability problems of the traditional APF, the improvement measures of improving the repulsive field function and inserting dynamic virtual target points are proposed. The improved artificial potential field repulsive function is introduced into the ACO, and the state transfer function is optimized to enhance the global convergence speed of the ACO and solve the problem of the original algorithm easily falling into the local optimum. Establishing 10×10 raster maps as the working environment for robot path planning, the optimal combination of parameters is derived through extensive experiments. The simulation results show that the improved ACO not only finds the optimal path for the leading robot, but also the path length and number of iterations are better than the traditional ACO. Finally, the combination of simulation verification based on graph theory and consistent formation control method finds a better path for multi-robot cooperative driving.

In future research, we will optimize the above methods more deeply for application to path planning problems with higher dimensionality and more complex environments.

Author Contributions: Formal analysis, D.L.; Investigation, Z.L.; Methodology, D.L.; Project administration, R.B.; Software, Z.L.; Supervision, R.B.; Writing—original draft, D.L. and Z.L.; Writing—review & editing, R.B. All authors have read and agreed to the published version of the manuscript.

Funding: This research was funded by China Scholarship Council: (2019)75.

Conflicts of Interest: The authors declare no conflict of interest.

References

1. Ajeil, F.H.; Ibraheem, I.K.; Azar, A.T.; Humaidi, A.J. Grid-based mobile robot path planning using aging-based ant colony optimization algorithm in static and dynamic environments. *Sensors* **2020**, *20*, 1880. [[CrossRef](#)] [[PubMed](#)]
2. Nazarahari, M.; Khanmirza, E.; Doostie, S. Multi-objective multi-robot path planning in continuous environment using an enhanced genetic algorithm. *Expert Syst. Appl.* **2019**, *115*, 106–120. [[CrossRef](#)]
3. Wang, D.; Chen, S.; Zhang, Y.; Liu, L. Path planning of mobile robot in dynamic environment: Fuzzy artificial potential field and extensible neural network. *Artif. Life Robot.* **2021**, *26*, 129–139. [[CrossRef](#)]
4. Kumar, A.; Kumar, P.B.; Parhi, D.R. Intelligent navigation of humanoids in cluttered environments using regression analysis and genetic algorithm. *Arab. J. Sci. Eng.* **2018**, *43*, 7655–7678. [[CrossRef](#)]
5. Hidalgo-Paniagua, A.; Vega-Rodríguez, M.A.; Ferruz, J.; Pavón, N. Solving the multi-objective path planning problem in mobile robotics with a firefly-based approach. *Soft Comput.* **2017**, *21*, 949–964. [[CrossRef](#)]
6. Duchoň, F.; Babinec, A.; Kajan, M.; Beno, P.; Florek, M.; Fico, T.; Jurišica, L. Path planning with modified a star algorithm for a mobile robot. *Procedia Eng.* **2014**, *96*, 59–69. [[CrossRef](#)]
7. Chen, Y.B.; Luo, G.C.; Mei, Y.S.; Yu, J.Q.; Su, X.L. UAV path planning using artificial potential field method updated by optimal control theory. *Int. J. Syst. Sci.* **2016**, *47*, 1407–1420. [[CrossRef](#)]
8. Gong, L.; Zhang, Y.; Cheng, J. Coordinated Path Planning Based on RRT Algorithm for Robot. *Appl. Mech. Mater.* **2014**, *494*, 1003–1007. [[CrossRef](#)]
9. Xu, X.; Cao, D.; Zhou, Y.; Gao, J. Application of neural network algorithm in fault diagnosis of mechanical intelligence. *Mech. Syst. Signal Processing* **2020**, *141*, 106625. [[CrossRef](#)]
10. Peng, J.; Huang, Y.; Luo, G. Robot path planning based on improved A* algorithm. *Cybern. Inf. Technol.* **2015**, *15*, 171–180. [[CrossRef](#)]
11. Gan, Y.; Zhang, B.; Ke, C.; Zhu, X.; He, W.; Ihara, T. Research on Robot Motion Planning Based on RRT Algorithm with Nonholonomic Constraints. *Neural Processing Lett.* **2021**, *53*, 3011–3029. [[CrossRef](#)]
12. Ma, Y.; Mao, Z.; Wang, T.; Qin, J.; Ding, W.; Meng, X. Obstacle avoidance path planning of unmanned submarine vehicle in ocean current environment based on improved firework-ant colony algorithm. *Comput. Electr. Eng.* **2020**, *87*, 106773. [[CrossRef](#)]
13. Orozco-Rosas, U.; Montiel, O.; Sepúlveda, R. Mobile robot path planning using membrane evolutionary artificial potential field. *Appl. Soft Comput.* **2019**, *77*, 236–251. [[CrossRef](#)]
14. Kovács, B.; Szayer, G.; Tajti, F.; Burdelis, M.; Korondi, P. A novel potential field method for path planning of mobile robots by adapting animal motion attributes. *Robot. Auton. Syst.* **2016**, *82*, 24–34. [[CrossRef](#)]
15. Das, M.S.; Sanyal, S.; Mandal, S. Navigation of Multiple Robots in Formative Manner in an Unknown Environment using Artificial Potential Field Based Path Planning Algorithm. *Ain Shams Eng. J.* **2022**, *13*, 101675. [[CrossRef](#)]
16. Hou, P.; Pan, H.; Guo, C. Simulation research for mobile robot path planning based on improved artificial potential field method recommended by the AsiaSim. *Int. J. Modeling Simul. Sci. Comput.* **2017**, *8*, 1750046. [[CrossRef](#)]
17. Akka, K.; Khaber, F. Mobile robot path planning using an improved ant colony optimization. *Int. J. Adv. Robot. Syst.* **2018**, *15*, 1729881418774673. [[CrossRef](#)]
18. Che, G.; Liu, L.; Yu, Z. An improved ant colony optimization algorithm based on particle swarm optimization algorithm for path planning of autonomous underwater vehicle. *J. Ambient. Intell. Humaniz. Comput.* **2020**, *11*, 3349–3354. [[CrossRef](#)]
19. Sangeetha, V.; Krishankumar, R.; Ravichandran, K.S.; Cavallaro, F.; Kar, S.; Pamucar, D.; Mardani, A. A fuzzy gain-based dynamic ant colony optimization for path planning in dynamic environments. *Symmetry* **2021**, *13*, 280. [[CrossRef](#)]
20. Tao, Y.; Gao, H.; Ren, F.; Chen, C.; Wang, T.; Xiong, H.; Jiang, S. A Mobile Service Robot Global Path Planning Method Based on Ant Colony Optimization and Fuzzy Control. *Appl. Sci.* **2021**, *11*, 3605. [[CrossRef](#)]
21. Luo, Q.; Wang, H.; Zheng, Y.; He, J. Research on path planning of mobile robot based on improved ant colony algorithm. *Neural Comput. Appl.* **2020**, *32*, 1555–1566. [[CrossRef](#)]
22. Han, Z.; Liu, S.; Yu, F.; Zhang, X.; Zhang, G. A 3D measuring path planning strategy for intelligent CMMs based on an improved ant colony algorithm. *Int. J. Adv. Manuf. Technol.* **2017**, *93*, 1487–1497. [[CrossRef](#)]
23. Jiao, Z.; Ma, K.; Rong, Y.; Wang, P.; Zhang, H.; Wang, S. A path planning method using adaptive polymorphic ant colony algorithm for smart wheelchairs. *J. Comput. Sci.* **2018**, *25*, 50–57. [[CrossRef](#)]
24. Liang, Y.; Wang, L. Applying genetic algorithm and ant colony optimization algorithm into marine investigation path planning model. *Soft Comput.* **2020**, *24*, 8199–8210. [[CrossRef](#)]
25. Gao, W.; Tang, Q.; Ye, B.; Yang, Y.; Yao, J. An enhanced heuristic ant colony optimization for mobile robot path planning. *Soft Comput.* **2020**, *24*, 6139–6150. [[CrossRef](#)]

26. Liu, J.; Yang, J.; Liu, H.; Tian, X.; Gao, M. An improved ant colony algorithm for robot path planning. *Soft Comput.* **2017**, *21*, 5829–5839. [[CrossRef](#)]
27. Chen, Y.; Bai, G.; Zhan, Y.; Hu, X.; Liu, J. Path planning and obstacle avoiding of the USV based on improved ACO-APF hybrid algorithm with adaptive early-warning. *IEEE Access* **2021**, *9*, 40728–40742. [[CrossRef](#)]
28. Liu, H.; Liu, F.; Zhang, X.; Guan, X.; Chen, J.; Savinaud, P. Aircraft conflict resolution method based on hybrid ant colony optimization and artificial potential field. *Sci. China Inf. Sci.* **2018**, *61*, 129103:1–129103:3. [[CrossRef](#)]
29. Park, S.O.; Lee, M.C.; Kim, J. Trajectory planning with collision avoidance for redundant robots using jacobian and artificial potential field-based real-time inverse kinematics. *Int. J. Control. Autom. Syst.* **2020**, *18*, 2095–2107. [[CrossRef](#)]
30. Sun, J.; Tang, J.; Lao, S. Collision avoidance for cooperative UAVs with optimized artificial potential field algorithm. *IEEE Access* **2017**, *5*, 18382–18390. [[CrossRef](#)]
31. Peng, Z.; Wen, G.; Rahmani, A.; Yu, Y. Distributed consensus-based formation control for multiple nonholonomic mobile robots with a specified reference trajectory. *Int. J. Syst. Sci.* **2015**, *46*, 1447–1457. [[CrossRef](#)]
32. Pan, Z.; Wang, D.; Deng, H.; Li, K. A virtual spring method for the multi-robot path planning and formation control. *Int. J. Control. Autom. Syst.* **2019**, *17*, 1272–1282. [[CrossRef](#)]
33. Wu, X.; Wang, S.; Xing, M. Observer-based leader-following formation control for multi-robot with obstacle avoidance. *IEEE Access* **2018**, *7*, 14791–14798. [[CrossRef](#)]
34. Mahmood, B.A.D.; Ghafil, H.; Jármai, K. Optimizing Heuristic Graph Formation with Application in Kinematic Synthesis of a Robot Arm with Revolute Joints. *J. Eng. Appl. Sci.* **2019**, *14*, 1976–1948.
35. Liu, D.; Zong, C.; Wang, D.; Zhao, W.; Wang, Y.; Lu, W. Multi-robot formation control based on high-order bilateral consensus. *Meas. Control* **2020**, *53*, 983–993. [[CrossRef](#)]
36. Wang, P.; Liu, P.; Chiclana, F. Multi-stage consistency optimization algorithm for decision making with incomplete probabilistic linguistic preference relation. *Inf. Sci.* **2021**, *556*, 361–388. [[CrossRef](#)]
37. Ebel, H.; Eberhard, P. A comparative look at two formation control approaches based on optimization and algebraic graph theory. *Robot. Auton. Syst.* **2021**, *136*, 103686. [[CrossRef](#)]
38. Yan, B.; Shi, P.; Lim, C.C.; Wu, C.; Shi, Z. Optimally distributed formation control with obstacle avoidance for mixed-order multi-agent systems under switching topologies. *IET Control Theory Appl.* **2018**, *12*, 1853–1863. [[CrossRef](#)]